ISSN 1027-4510, Journal of Surface Investigation: X-ray, Synchrotron and Neutron Techniques, 2023, Vol. 17, No. 2, pp. 338–351. © Pleiades Publishing, Ltd., 2023.
Russian Text © The Author(s), 2023, published in Poverkhnost', 2023, No. 3, pp. 23–39.

Surface Nanorelief of Thin Films of Al–Mn and Al–Ni Alloys in the Case of Ion-Assisted Deposition on Glass

I. I. Tashlykova-Bushkevich[a, *] and I. A. Stolyar[b]

[a] *Belarusian State University of Informatics and Radioelectronics, Minsk, 220013 Belarus*

[b] *Belarusian State University, Minsk, 220050 Belarus*

**e-mail: iya.itb@bsuir.by*

Received July 22, 2022; revised September 9, 2022; accepted September 9, 2022

Abstract—The patterns of structure formation and the wetting of thin films of aluminum and its Al–2.1 at % Mn and Al–1.4 at % Ni alloys deposited onto glass substrates with assistance by self ions are studied. Nanoscale and microsized topographic inhomogeneities on the film surface are characterized by scanning probe microscopy (SPM) and scanning electron microscopy (SEM) and their wetting characteristics are measured by the sessile-drop method. Within the profile and topographic approaches to the analysis of SPM images, a set of discrete roughness parameters supplemented by dimensionless complex parameters (ψ and k) and probability-density-function parameters of the protrusions/depressions of the surface nanorelief is used. The proposed hybrid research parameter k characterizes the shape of nanorelief profile irregularities, is comprehensible, and relates the amplitude to the roughness step. The system of nine selected parameters is shown to be informative for estimating the roughness and irregularity of the local structure of the film surface in transverse and longitudinal cross sections, which makes it possible not only to numerically study the structural and morphological changes upon the alloying of aluminum, but also to determine quantitative relationships that relate the microgeometry of the film surface to the film deposition conditions. The effect of the initial relief of the glass substrate on the parameters of film surface inhomogeneities that have the shapes of submicrometer cones and local protuberances is revealed. The Gaussian distribution of the film nanoreliefs of aluminum and its alloys over the surface area is obtained, and the film surfaces can be considered as an implementation of a random normal process. The frequency distributions of the microdroplet fraction over particle sizes are lognormal functions. A correlation is found between the roughness parameters of the films and the size and density of microparticles of the droplet fraction. It is found that the deposition of Al-containing films reduces the hydrophilicity of the surface of the film–glass substrate system. Upon the alloying of aluminum, the degree of morphological inhomogeneity of the film surfaces and their wettability decrease. The homogeneous regime of film wetting with water and its dependence on the material, the morphology, and the homogeneity of the chemical composition of the surface are discussed.

Keywords: ion-assisted deposition, scanning probe microscopy, scanning electron microscopy, wettability, Al–Mn alloys, Al–Ni alloys

DOI: 10.1134/S1027451023020179

INTRODUCTION

At present, considerable attention is paid to studying the mechanisms of the formation and modification of the structure and properties of thin metal films obtained by ion-beam methods with the use of self ions, which are used as light-reflecting, hardening, and conductive coatings. Ion-beam assisted deposition techniques that are of interest for thin-film coatings [1–3] are promising for the synthesis of optical metallic films on dielectric substrates for modern devices of microelectronics and nanoelectronics, as well as for solar photovoltaics. Substrate glasses are in great demand for many applications, including the preparation of samples for laboratory research. For example, high performance solar cells are fabricated both on metallic substrates and on glass and Al_2O_3 substrates [4]. The development of theoretical foundations for the surface engineering of metal coatings under conditions of nonequilibrium solidification in the case of the influence of ion beams of a material requires understanding the influence of the conditions for depositing metal films on the structural state of surface layers of the coating–substrate system, which largely determines the physical-chemical and operational properties of coatings, including their conductive, corrosion, and reflective properties, and the degree of hydrophilicity/hydrophobicity of the sample surface [1–3].

In recent years, the methods of statistical physics and fractal analysis [5–7] have been increasingly used to describe the nanostructure and microstructure of

deposited films, which make it possible to generalize the available data and to reveal regularities in the formation of the surface relief of coatings under nonequilibrium conditions of the growth process. In particular, special attention is paid to thin films with a thickness from a few to tens of nanometers, the properties of which depend on the coating thicknesses and the choice of substrate material [8, 9]. However, the question of a universal set of statistical roughness parameters that most fully describe the degree of surface-structure ordering and its relationship with the conditions for the preparation of samples and their properties remains open today despite a fairly large number of standardized generally accepted parameters [10, 11]. Many experts point out (for example, in [12, 13]) that there is no unified approach to roughness assessment in world practice, and they are often limited to measuring and analyzing only the roughness-height parameters when studying films and coatings, despite the fact that they do not provide information about the geometry and the step of surface profile unevenness. According to the current level of research, it is considered relevant to use integral and differential distribution functions of rough surfaces that are random for an informative description, in addition to discrete parameters. At the same time, the search for correlations between topographic parameters and additional complex roughness parameters is ongoing [13–18]. In theoretical calculations, the real profile can be replaced by sinusoidal, sawtooth, and other profiles. For example, a model was developed in study [17] devoted to the issues of water wetting control of aluminum-alloy samples, in which the real surface profile with an artificially created relief is replaced by a sawtooth one and it is proposed to use the height-to-width ratio of the peaks of neighboring sawtooth surface structures as a parameter to establish the relationship between the surface microrelief and the volume of a water droplet penetrating into surface depressions.

This study is aimed at analyzing the patterns of structure formation and the wetting of thin films of aluminum and its Al–2.1 at % Mn and Al–1.4 at % Ni alloys deposited onto glass substrates using the method of self-ion assisted deposition (SIAD). During ion-assisted deposition, a metallic film is formed under conditions of ultrafast cooling rates, since the crystallization rate (cooling of cascades) reaches 10^{12}–10^{13} K/s [19]. During the formation of a thin-film coating, the vacuum deposition of a neutral fraction of the metal is accompanied by irradiation of the ionized fraction of the same metal with self ions [20, 21]. The choice of aluminum and Al–Mn and Al–Ni alloys is determined by the prospect of expanding the scope of application of thin-film structures based on aluminum as optical films and frontal contacts of solar cells [3, 22–24]. The advantages of aluminum alloys that have relatively low melting points are relatively high hardness values, good strength, ductility, and high corrosion resistance. It is well known that the microstructure of aluminum alloys directly depends on the introduced additives capable of increasing the thermal stability of the material, inhibiting recrystallization processes and, consequently, leading to stabilization of the film structure, including the morphology of their surface. Therefore, it is extremely important to determine the degree of influence of alloying elements on the structural and morphological characteristics of films when using aluminum films and in the case of controlling their physical-chemical and mechanical properties.

In this study, scanning probe microscopy (SPM) together with scanning electron microscopy (SEM) are used in a comprehensive study of the morphology and topography of metal film surfaces, including the roughness in the nanometer and micrometer ranges. For a quantitative description of the surface structure, the discrete topography characteristics are measured in accordance with the roughness parameters defined by the International Organization for Standardization (ISO) (transverse (height) and longitudinal (step) nanorelief characteristics) and a parametric function of the probability density function of the heights of protrusions/depressions. In this study, we statistically process the parameters of local elements of the topographic structure of the surface profiles taking into account the aperiodicity of structural components of the film surface morphology and calculate an additional research parameter of the hybrid coefficient [25–27] reflecting the change in the shape of the film-nanorelief-profile unevenness during the alloying of aluminum, which is important for diagnostics of the surface quality of the film–substrate system. The statistical methods of analysis are also used for processing the SEM images. Since the composition of the material and the conditions of ion-assisted deposition directly affect the structure of the films and, consequently, their properties, the sessile-drop method is used to measure the contact angle as a sensitive indicator of the state of solid surfaces. Frequently, the free surface energy characterizing physical-chemical phenomena, such as the wetting, adhesion, adsorption, and dispersion, is used to assess the operational and protective properties of solid materials [28]. Given that the free surface energy of solid materials cannot be measured directly, the contact angle of surface wetting by various liquids is analyzed. This clearly demonstrates the practical significance of the wetting phenomenon.

EXPERIMENTAL

Films of aluminum (99.995) and its Al–2.1 at % Mn and Al–1.4 at % Ni alloys were obtained by self-ion-assisted deposition onto glass substrates using a resonance ion source of vacuum arc plasma [20] at an accelerating voltage of 3.0 kV and a pressure of about 10^{-2} Pa in the working chamber. The electrodes used in the ion source, which simultaneously generates a

neutral flux of atoms and a flux of ions of the deposited metal, were made of material of the deposited coating (aluminum and its alloys). The strength of the ion current and its density were 100 μA and 5.1 μA/cm^2, respectively. The ratio of the ion-flux density to the flux density of neutral atoms j_i/j_A was 0.1–0.4 and corresponded to growth of the coating on the substrate. The coating-deposition times were 6 h for the Al–Ni alloy, 9.1 h for the Al–Mn alloy, and 10 h for Al. Since the rate of metal deposition is about 0.1–0.2 nm/min, the average film thicknesses were 50 nm for the Al–Ni alloy, 80 nm for the Al–Mn alloy, and 90 nm for the aluminum coating.

To visualize the nanostructure and surface nanorelief of films by SPM, we used an NT-206 atomic force microscope (AFM) [29] with the SurfaceScan control software package. Probes of the CSC-38 brand were used. The 20 × 20-μm images obtained in the contact mode in air were three-dimensional digital images of the surface roughness and were processed using filters in the SurfaceXplorer and SurfaceView software packages (ODO Microtestmashiny, Belarus [30]).

Six roughness parameters were used in a quantitative description of the topography of the films, which were determined according to the basic standards (GOST 25142-82 as amended on January 30, 2017). These are four amplitude parameters (arithmetic-mean roughness R_a, root-mean-square roughness R_q, profile skewness R_{sk}, and profile kurtosis R_{ku}) and two step parameters (average step S between profile protrusions and average step S_m of profile irregularities). In addition, the parameter called "profile irregularity heights over ten points" was defined using the designation R_{10z} proposed by a research group in [13, 16]. The R_{10z} parameter was included until recently in GOST 25142-82, but now excluded from the current version of the standards for roughness parameters, and its former designation (R_z) is used for another parameter. Nevertheless, a considerable amount of statistical data on the R_{10z} parameter has been accumulated along with other parameters, and it continues to be widely used in practice. The following dimensionless complexes were also calculated: parameter $\psi = S/S_m$ of the ratio of step parameters of the profile [16, 31]; and hybrid research coefficient $k = R_{10z}/S$ [25–27], which depends on the amplitude and step of the nanorelief roughness.

Parameter R_a of the arithmetic-mean roughness is considered statistically stable; it was chosen to control the correctness of the results of the analytical method for processing AFM images, which is described in this study. The arithmetic-mean surface roughness of each sample was determined from four to five images. After that, the site was selected, for which the measured R_a value was as close as possible to a certain average value of this parameter. Since the SurfaceXplorer software does not calculate R_{10z}, and the roughness step parameters are measured only for an individual profile, we developed and implemented an algorithm for the statistical processing of AFM data for a topographic analysis of the sample surface with use of the OriginPro software package and MS Excel spreadsheets when calculating the average values of the R_z, S, and S_m parameters determined by the standard formulas [32] using the method of counting intersections with the level of profile quantization. For each surface, eleven profilograms were recorded and processed. To gain the specified accuracy and reliability of the measurement results when assessing microtopographic parameters, the deviation of the R_a value calculated analytically during profile and topographic analyses from the value of this parameter measured in the SurfaceXplorer software package was 5–15%.

The height of irregularities (peaks/depressions) relative to the middle line, i.e., the base line for calculating the roughness, was chosen as a parametric function that characterizes the topography. The experimentally determined frequency polygons $f(z)$ were compared with the theoretical probability density function of the normal distribution in the OriginPro software package.

SEM analysis was carried out using a LEO1455VP microscope with an HKL CHANNEL5 attachment in the mode of recording backscattered electrons at an accelerating voltage of 20 kV. The secant method [33] was used to determine the mean size $\bar{D}$, volume fraction V, and specific surface area S_{sp} of the boundaries of microparticles of the droplet fraction on SEM images by using MS Excel spreadsheets with standard formulas. The measurement error was about 15%.

Wetting of the surface of the film/glass substrate structures obtained by the SIAD method by distilled water (GOST R 58144–2018) was characterized by the value of the equilibrium contact angle θ. The measurements were performed by the sessile-drop method after applying a drop in the device described in [34] at an environment temperature of 20 ± 3°C. The drop volume was 9.3 μL. The stabilization time of the sample–droplet system was 60 s. The measurement error was about 5%.

RESULTS AND DISCUSSION

Figure 1 shows typical surface-relief images of the glass substrate and thin films of Al and its Al–2.1 at % Mn and Al–1.4 at % Ni alloys deposited on glass. According to the AFM data, the morphology of the glass substrate is of the fine-component type (Fig. 1a), in which the spread of typical surface-relief protrusions with a height of 20 μm does not exceed 1 nm. The investigated surface of aluminum films and its alloys is rough and is characterized by irregularities of various geometric types with varying degrees of inhomogeneity depending on the elemental composition

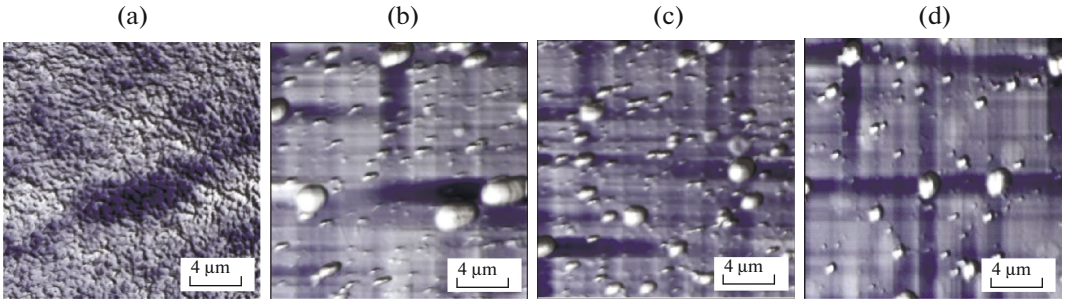

Fig. 1. Atomic-force-microscopy images of the surface nanoreliefs of (a) the initial glass substrate and thin films of (b) aluminum and its (c) Al–2.1 at % Mn and (d) Al–1.4 at % Ni alloys deposited onto glass.

of the samples and the time of ion-assisted deposition onto glass (Fig. 1). The arithmetic-mean roughness R_a values measured for different coatings in a scanning window 20 × 20 μm in size ranged from 17 to 32 nm and are given in Table 1. Table 1 also shows other parameters that characterize the morphological features of the glass and film surfaces. From a scientific perspective, correlations between roughness parameters are of great interest. The difference between the amplitude parameters R_a and R_q fluctuates between 1.6 fold and 1.8 fold. As can be seen from Table 1, the higher the degree of roughness of the alloy film, the greater the root-mean-square (rms) roughness R_q. Table 1 also includes complex parameters ψ and k, the calculation of which is described below.

To approximate the shape of the surface-profile irregularities and to compare the samples with each other, additional statistical analysis of the nanorelief of metallic films deposited onto glass was performed using the data of AFM measurements. The general algorithm described below for profile and topographic analyses was applied to the sample of an Al–Ni alloy coating, a typical AFM image of which is shown in Fig. 1d. In the initial stage, a raster scan of the obtained AFM image of a section of the sample surface is performed manually as follows. A sequence of closely spaced parallel lines (trajectories) is selected along the X direction for nanorelief profiling (Fig. 2a). Movement along the Y axis is carried out with such a Δy step that the average R_a values determined for individual profiles using the SurfaceXplorer software package coincide with the R_a value measured for the entire area of 20 × 20 μm (SurfaceXplorer) within an error margin of 5–15%. It was found that this level of accuracy is achieved with $\Delta y = 2$ μm, i.e., it is sufficient to carry out measurements for a set of eleven horizontal scanning lines (Fig. 2b). Figure 2c shows cross-sectional profiles $z(x,y)$ of the surface of the Al–1.4 at % Ni alloy film, which are obtained by scanning the AFM image shown in Fig. 2b along the lines with serial numbers 4, 8, and 9. This example clearly demonstrates that the roughness parameter widely used in AFM analyses as the main roughness parameter R_a does not contain information about the surface profile shape. In particular, areas with different distributions of irregularities of different shapes over heights can have close arithmetic-mean roughness values in the range from 9.5 to 10.6 nm (Fig. 2c).

Figure 3 schematically shows a typical nanorelief profile of the film, which has a pronounced irregular shape. According to state standards, the amplitude roughness parameters are determined relative to the middle line. In the section of the basal length, the middle line of the profile looks like a straight line. In practice, the basal length l in the AFM measurements coincides with the side of the square area of the scanning window in which the surface roughness is estimated. The lines of protrusions and depressions are equidistant from the middle line (Fig. 3a). Its position z_{mean}, which is determined in the metrology of rough surfaces using the least squares method, was numerically measured using the SurfaceXplorer software package. Figure 3a graphically illustrates the procedure for analytical calculation of the following averaged roughness parame-

Table 1. Values of the parameters describing the morphology, the roughness, and the wetting of the glass substrate for films of Al and Al–2.1 at % Mn and Al–1.4 at % Ni alloys deposited onto glass

Sample	t, h	R_a, nm	R_q, nm	ψ	k, $\times 10^{-2}$	$\bar{D}$, μm	V, %	S_{sp}, 10^{-2} μm^{-1}	θ, deg
Glass	–	0.17	0.22	1.23	0.04	–	–	–	22.0
Al	10.0	31.51	51.52	1.23	2.14	0.88	5.45	20.21	73.20
Al–Mn	9.1	23.87	39.92	1.27	3.19	0.96	3.82	13.01	74.40
Al–Ni	6.0	17.09	30.69	1.28	2.13	0.46	1.77	12.68	81.30

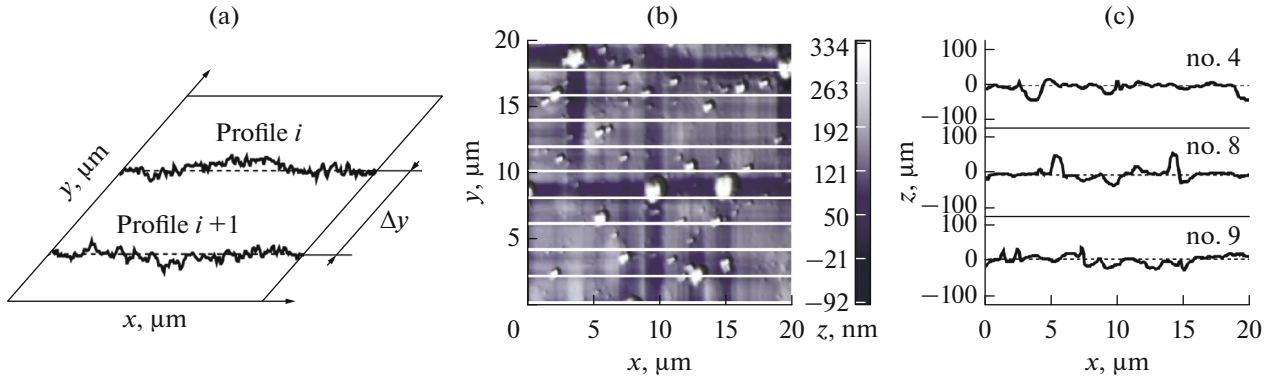

Fig. 2. Algorithm for statistical analysis of the characteristics of the surface topography of a metallic film of Al–1.4 at % Ni alloy: (a) scanning trajectories of the AFM image, in which index i indicates the scanning profile number counted from the top edge of the image and changes from 1 to 11; (b) the AFM image with selected lines of surface scanning; (c) cross-sectional profiles of the surface nanorelief measured for trajectories no. 4, no. 8, and no. 9 with arithmetic-mean roughness values R_a of 9.46, 10.61, and 10.29 nm, respectively.

ters: profile irregularity heights R_{10z}, average step S of local protrusions of the profile, and average step S_m of profile irregularities. According to the definition, R_{10z} characterizes the average height of the largest irregularities, which is determined over ten local points of profile minima and maxima within the basal length as a mean between the five highest points (protrusions or peaks) and the five lowest points (depressions) of the relief by the following formula [32]:

$$R_{10z} = \frac{1}{5}\left(\sum_{i=1}^{5}\left|z_{\max i}\right| + \sum_{i=1}^{5}\left|z_{\min i}\right|\right),$$

where $z_{\max i}$ is the height of the ith largest protrusion, and $z_{\min i}$ is the depth of the ith largest depression. The average step S of the local protrusions of the profile equals the average distance S_i between adjacent peaks of characteristic irregularities within the basal length in accordance with the following formula [32]:

$$S = \frac{1}{n}\sum_{i=1}^{n} S_i,$$

where n is the number of local peaks along the profile. Only those neighboring peaks are taken into account, the height difference of which is no less than 10% of the maximum profile irregularity height designated as R_z in the current version of the state standard [32]. This extreme profile parameter R_z characterizes the maximum height of the profile and is calculated as the distance between the lines of protrusions and depressions (Fig. 3a). A continuous material of the film is located below this layer. Using this height parameter, one can estimate the thickness of the rough (sometimes called "perturbed" [35]) surface layer partially filled with the material. It is in the rough layer that the surface topography changes. It was found that R_{zi} for films of aluminum and its alloys with manganese and nickel exceeds, as a rule, the average thickness of the films when scanning along individual trajectories and the average R_z values equal 180.1, 206.0, and 107.3 nm, respectively.

The average step of the profile S_m irregularities is defined as an arithmetic-mean of the step of profile S_{mi} irregularities within the basal length by the following formula:

$$S_m = \frac{1}{m}\sum_{i=1}^{m} S_{mi},$$

where m is the number of middle line sections containing a depression and a protrusion along the middle line of the surface profile. The meaning of S_m is explained in Fig. 3a. It was found that the average step of profile S_m irregularities of films of aluminum and its alloys, which can be considered equivalent to the average wavelength λ_a of the profile [15], lies in the range of about 2.0–5.8 μm.

The ratio of the above profile step parameters determined in the SurfaceXplorer software package allows us to calculate parameter $\psi = S/S_m$, which characterizes the profile spectrum width. The ψ values experimentally found for the glass substrate and the aluminum film coincide and equal 1.23 (Table 1). For the alloys, the ψ value is approximately the same and only 4% higher than the initial value calculated for the aluminum film, and equals 1.28 on average.

For each sample, hybrid research parameter k that characterizes the spatial inhomogeneity and shape of the surface nanorelief of the films was calculated using the described analysis procedure. The calculated k values are given in Table 1 to compare the surface microgeometry of the samples. Upon increasing the time of film deposition, a nonmonotonic change in the hybrid parameter is observed with an increase in the surface roughness. It was experimentally determined that the

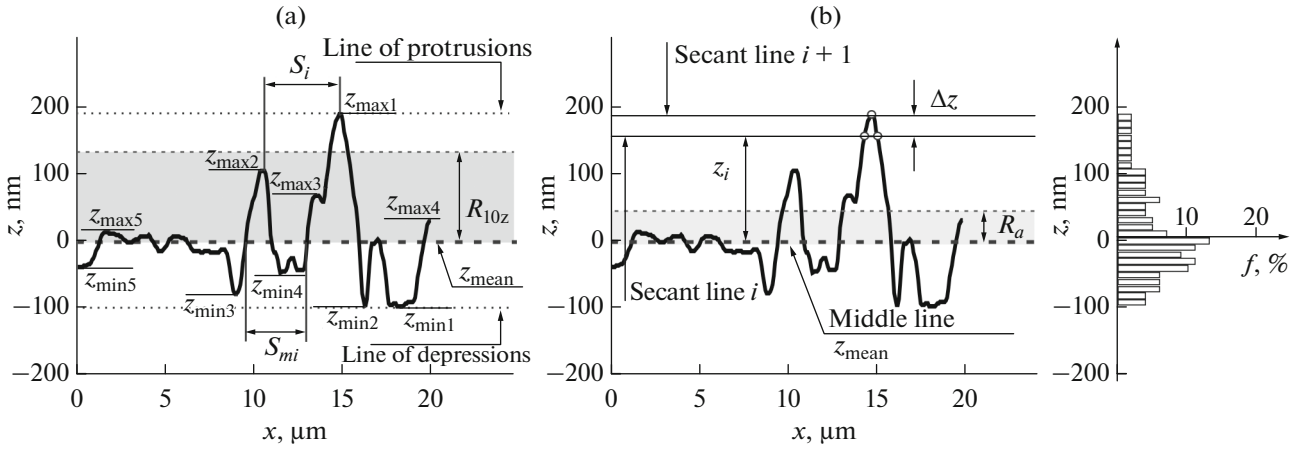

Fig. 3. Determining (a) the standardized roughness parameters R_{10z}, S, and S_m, and (b) the frequency distribution of the protrusions/depressions of the film surface cross-sectional profile with $z_{\text{mean}} \approx 0$, $|z_{\max i}| > |z_{\max i+1}|$, $|z_{\min i}| > |z_{\min i+1}|$, and $i = \overline{1,5}$.

values of this parameter for films of aluminum and its alloy with nickel practically coincide and equal about 2.14, which is more than 50 times higher than the value determined for glass. For the Al–Mn alloy, the k parameter increases by 50% compared to that of the other films and equals 3.19.

In addition to determining the roughness parameters, investigation of the spatial inhomogeneity and statistical characteristics of the film-surface topography also included a procedure for constructing the distribution histograms of protrusions/depressions of irregularities both for a single profile and for the entire scanned surface area. Figure 3b graphically illustrates the method used for determining the frequency composition f of the roughness of a single surface profile by counting the number of intersections of the profile by auxiliary secants drawn parallel to the middle line of the surface profile with a step Δz within the basal length l in accordance with the following formula [32]:

$$R_a = \frac{1}{l}\int_0^l |z(x)|\,dx \approx \frac{1}{n}\sum_{i=1}^{N}|z_i - z_{\text{mean}}| = \frac{\sum_{i=1}^{N}|z_i - z_{\text{mean}}|\,n_i}{\sum_{i=1}^{N} n_i},$$

where $z(x)$ is the function of deviations of the surface profile from the middle line, n is the number of profile partitions, z_i is the deviation of the profile in an arbitrary section, n_i is the number of intersections of the auxiliary ith secant at height z_i, and N is the number of secants. Taking into account the experimental values of parameter R_z, which specifies the maximum height of profile irregularities, a satisfactory degree of accuracy of the analytically calculated R_a value was achieved with a step of $\Delta z = 10$ nm.

Figure 4 shows an example of the analytically measured frequency composition of the surface of the Al–Ni alloy film deposited onto glass with $U = 3.0$ kV and $t = 6$ h. The profile analyses illustrated in Figs. 4a–4c were performed for the nanoreliefs constructed along the selected lines of scanning of the Al–1.4 at % Ni alloy film (Fig. 2c). It should be noted that the SurfaceXplorer software package does not allow one to construct a histogram for an individual cross-sectional surface profile. Assuming that the distribution function of the material (metal/alloy) over the height of the rough surface layer of the film is close to a normal distribution, the experimental histograms were approximated by a Gaussian distribution. The root-mean-square deviation σ of the surface point heights determined during fitting in the OriginPro software package can be considered as a statistical parameter that characterizes the irregularity of the relief, i.e., the degree of its heterogeneity or the degree of its deviation from the planar shape. As can be seen from Figs. 4a–4c, the larger the σ value, the greater the surface-profile wrinkling (Fig. 2c) and the more satisfactorily the empirical distribution is described by a Gaussian curve. The Gaussian curve indicates how often one or another local protrusion/depression is repeated in the profile. For example, the most common height coincides with the middle line of the profile. Figure 4d gives the results of an analytical topographic analysis of the film surface shown in Fig. 2b.

Figure 5 shows the distribution histograms of the nanorelief protrusions/depressions of the glass substrate and films of Al and its alloys, whose AFM images are shown in Fig. 1, which are obtained using the SurfaceXplorer software package. It is established that the empirical frequency distributions $f(z)$ of the

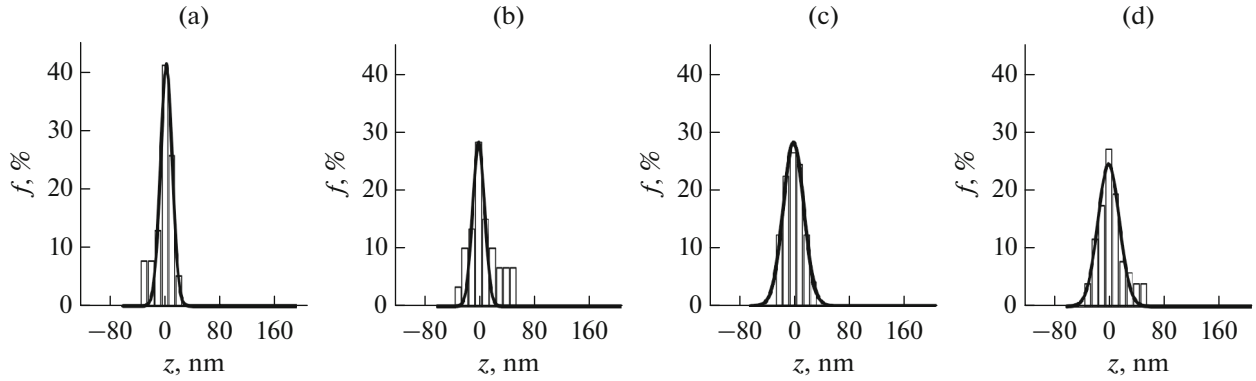

Fig. 4. Analytically calculated distribution histograms of the surface nanorelief protrusions/depressions of films of the Al–1.4 at % Ni alloys for the cross-sectional nanorelief profiles along scanning lines (a) no. 4, (b) no. 8, and (c) no. 9, and (d) for the entire surface (the peak is located at −2.01 nm). The measured (analytically) R_a and σ (OriginPro) values are (a) 8.72 and 8.45, (b) 15.83 and 8.52, (c) 10.60 and 14.85, and (d) 18.28 and 15.30 nm, respectively.

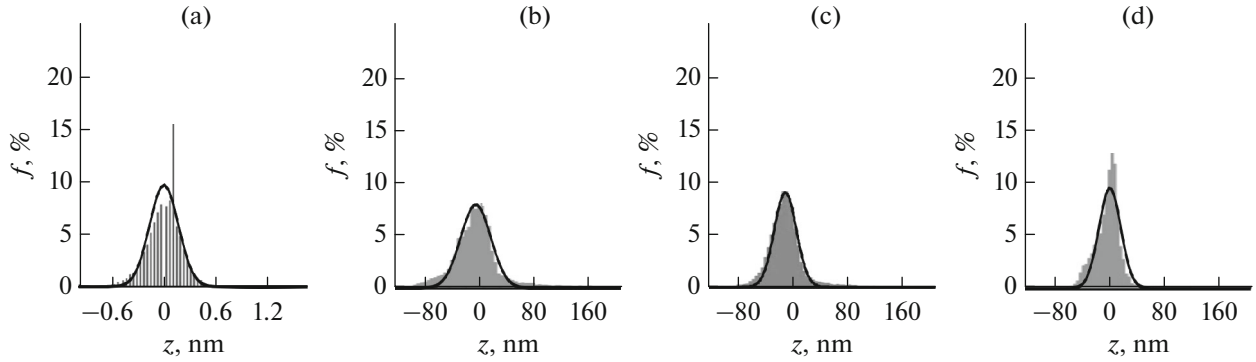

Fig. 5. Distribution histograms of the surface nanorelief protrusions/depressions of (a) the initial glass substrate and thin films of (b) Al and its (c) Al–2.1 at % Mn and (d) Al–1.4 at % alloys deposited onto glass, which are obtained using the SurfaceXplorer software package and fitted with a Gaussian distribution in the OriginPro software package.

profile ordinates of the studied surfaces are unimodal functions and qualitatively agree with a normal distribution. Parameters describing the histograms after numerical processing in the OriginPro software package and the results of fittings by a Gaussian distribution are given in Table 2. It was found that the degree of deviation of the surface-relief distribution over the heights from the normal one is at a minimum level for the glass substrate ($R_{sk} = 0$ and $R_{ku} = 3$). For films, an increase in the R_{ku} parameter with an increase in R_{sk} is observed upon increasing the time of film deposition. The following scale dependence on the area of surface analysis is revealed when comparing Figs. 5d and 4: the height of the final histogram naturally decreases upon averaging over the entire surface during topographic analysis.

According to the obtained SEM images shown in Figs. 6, thin films of Al and the Al–2.1 at % Mn and Al–1.4 at % Ni alloys deposited onto glass are continuous coatings without strains. The presence of microparticles of the droplet fraction from the coating applied on the surface of the films is explained by the presence of drops of the cathode material in plasma flows generated by the arc. Most microparticles are spherical in shape. The partial flattening of some microparticles, which indicates that they got to the surface of the film in the molten state—can increase their adhesion to the surface of the films. Table 1 gives the results of the statistical analysis of SEM images by the secant method. As can be seen from Table 1, the microparticles of the droplet fraction have the smallest size and the smallest volume fraction (0.46 μm and 1.77%) on the surface of the Al–Ni alloy film comapared to the other films when deposited with a relatively short film-deposition time. It was found that the values of the specific surface area S_{sp} of microparticle boundaries on the surface of films of the Al–Mn and Al–Ni alloys are practically the same, while their size and volume fraction in the case of an alloy with manganese are approximately twice higher (0.96 μm and 3.82%). This indicates a lower surface density of the microparticles of the droplet fraction on the surface of the Al–Mn alloy film, which is associated, among other things, with the embedding of previously

Table 2. Values of the parameters describing the distribution histograms of the protrusions/depressions of the surface nanorelief of the initial glass substrate with deposited films of Al and Al–2.1 at % Mn and Al–1.4 at % Ni alloys (Fig. 5)

Material		SurfaceXplorer			OriginPro				
sample	t, h	R_{sk}	R_{ku}	z_{mean}, nm	z_c, nm	f_{max}, %	A, arb. units	σ, nm	COD (R^2)
Glass	–	–0.40	4.03	–0.1	–0.02	9.72	4.04	0.17	0.89
Al	10.0	1.72	10.11	–3.21	–4.57	7.87	432.97	22.0	0.98
Al–Mn	9.1	2.76	15.64	–4.01	–10.39	8.92	356.44	15.95	0.98
Al–Ni	6.0	–0.80	7.35	–2.07	1.0	9.43	371.90	15.77	0.95

deposited microparticles when the coating grows in the course of film deposition.

The frequency distribution curves of microparticle sizes (Fig. 6) demonstrate a positive deviation from the normal law and are described by lognormal curves with a coefficient of determination COD (R^2) of 0.84–0.98. Figure 3 shows the following statistical model parameters: modal value z_{max} that corresponds to the lognormal distribution maximum, and the median (z_{med}) and mean ($\langle z \rangle$) values. It was found that it is preferable to use the $\langle z \rangle$ values as a characteristic parameter for the size of microdroplets, since the error margins satisfactorily overlap in this case for determining the mean diameter of microparticles by the secant method and by constructing the lognormal distribution function. The statistical analysis of SEM data makes it possible to identify the size group of microparticles of the droplet fraction, which made the greatest contribution to the formation of the film surface relief. It was found that the largest fraction (60–70%) of microparticles on the film surface has a size of up to 0.6 μm. Upon increasing the deposition time from 6 to 10 h, the fraction of larger microparticles with a diameter of 0.6–1.0 μm increases, and the area under the lognormal distribution curve remains almost unchanged. The value of the variation coefficient CV that characterizes the degree of data uniformity exceeds 33% for the alloy films (the case of a homogeneous set) compared to the aluminum film, for which a more uniform size distribution of microparticles was found ($CV = 31.2\%$).

As was found from studying the wetting of samples with distilled water, films of aluminum and its alloys exhibit hydrophilic properties. The shape of the droplet applied on the film surface is shown in Fig. 7a. The deposition of films of Al and its Al–2.1 at % Mn and Al–1.4 at % Ni alloys on the glass substrate at $U = 3.0$ kV reduces the degree of hydrophilicity of the glass surface partially wetted with water ($\theta = 22.0°$). In the case of metallic films, the equilibrium contact angle increases and reaches the largest value (81.30°) for the alloy of aluminum with nickel (Table 1).

The thin-film coatings in this study were formed by the SIAD method, the distinctive advantage of which consists in using the ions of the deposited metal as assisting ions that allow one to obtain coatings without inert-gas impurity inclusions. During ion-beam deposition, the energy of deposited particles ranges from a few to tens of electron volts and does not decrease during film deposition, since the process is conducted in high vacuum. The use of the SIAD method provides improved the properties of the films, including good adhesion of the coating to the substrate without any restrictions on the composition of the deposited layers and their thickness [36]. Both refractory and low-melting metals and alloys can be used as a cathode plasma-forming material, which make it possible to synthesize films of various compositions. During film deposition, the crystallization rate upon cooling the

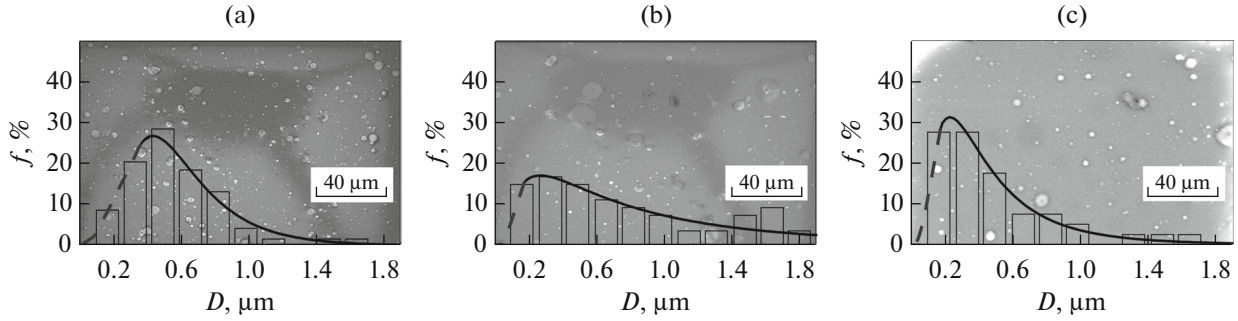

Fig. 6. Typical SEM images of the surface of thin films of (a) Al and its (b) Al–2.1 at % Mn and (c) Al–1.4 at % Ni alloys deposited onto a glass substrate with the corresponding size-distribution histograms of microparticles of the droplet fraction.

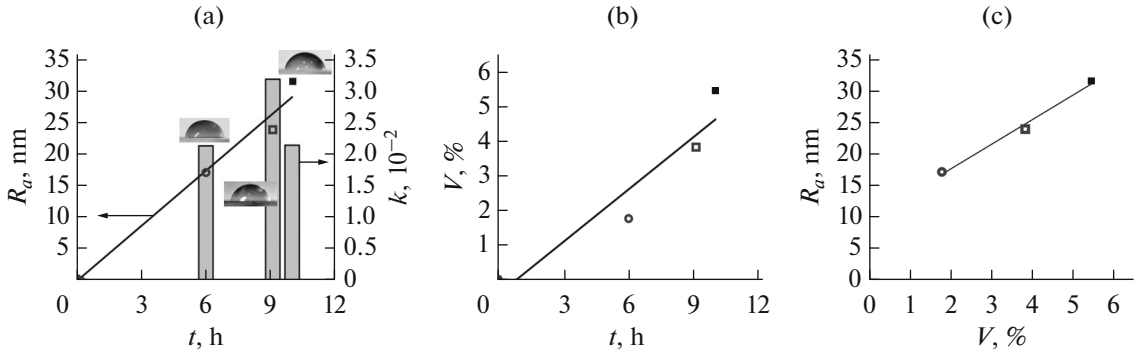

Fig. 7. Correlation between (a) topographic parameters R_a and k, and (b) volume fraction V of particles of the microdroplet fraction and (●) the time of deposition of the coatings on the glass substrate, as well as (c) the dependence of R_a on V for thin films of (■) Al (t = 10 h) and its (○) Al–2.1 at % Mn (t = 6 h) and (□) Al–1.4 at % Ni (t = 9.1 h) alloys. The shape of the droplets of distilled water on the film surfaces is shown. Empirical values of the coefficients of equation $y = ax + b$ and COD (R^2) for data fitting are as follows: (a) a = 2.92, b = –0.17, and COD = 0.98; (b) a = 0.50, b = –0.37, and COD = 0.90; (c) a = 3.89, b = 9.83, and COD = 0.99.

atomic collision cascades reaches 10^{12}–10^{13} K/s [19], which is much higher than the crystallization rates obtained, for example, in the case of high-speed crystallization from the liquid phase (10^6 K/s) [37], and the alloying component concentrations sufficient for simulating the properties of alloys do not exceed a few atomic percent. This stimulates the study of structure formation patterns in slightly alloyed aluminum alloys modified by ion-beam methods. Hence, the synthesis of materials under nonequilibrium conditions with ultrafast cooling rates allows one to develop aluminum alloys with unique physical and chemical properties that cannot be achieved by traditional synthesis and heat-treatment methods. In particular, the surface morphology of films deposited by ion-plasma sputtering plays an extremely important role in controlling the set of surface properties of coatings, which are determined by the structure of the surface layers of the coating/substrate system, including the surface topography, rather than by the characteristics of the material as a whole.

It follows from the results obtained in this study that the effect of the initial substrate relief on the formation of the morphology of thin films is revealed when analyzing the longitudinal roughness parameters. The proportion of step parameters ψ of the metallic film profiles slightly differs from the value (ψ = 1.23) determined for the glass substrate (Table 1). Since ψ > 1, this indicates that the rough surface of both glass and metallic films cannot be considered as a sinusoidal profile (ψ = 1). The analysis of the ratio R_q/R_a of the transverse parameters leads to the same conclusion. It is believed that root-mean-square roughness R_q is an alternative parameter to roughness R_a that characterizes the average height of the profile irregularities and, to the fullest extent, the profiles described by random functions. In the case of a coating with a sinusoidal profile, these parameters differ insignificantly, and $R_q = 1.11R_a$ according to the theory [38]. In the present study, if the glass substrate does not have a pronounced relief, then the R_q/R_a ratio for glass is 1.29 (Table 1), i.e., the well-known relation $R_q = 1.25R_a$ valid for a Gaussian random surface is fairly well satisfied [38]. Therefore, it seems logical that the experimentally determined fact that averaged amplitude roughness parameters, such as the skewness and kurtosis of the distribution density of the surface profile ordinates, are close to the theoretical values for a normal random surface profile in the case of a glass substrate ($R_{sk} = 0$ and $R_{ku} = 3$). However, the cross-sectional surface relief of the films of aluminum and its alloys does not repeat, at first glance, the relief of the glass substrate. Firstly, the R_q value is 80% higher than the R_a value, though the surface roughness is at a minimum level in a thin film of the Al–Ni alloy compared to other samples. At the same time, the difference between these height parameters is less significant for films of the Al–Mn alloy and pure aluminum, and equals about 65%. Moreover, if we take into account the asymmetry of the histogram of the surface of the Al–Ni alloy film in the region of the frequency distribution of depressions, then we find that the results of AFM analysis are in good agreement and indicate that the film grows in islands [39] by the Volmer–Weber mechanism. Secondly, if a film of the Al–Ni alloy with a thickness of about 50 nm has comparatively deep depressions ($R_{sk} = -0.8$), then a positive skewness ($R_{sk} = 1.72$–2.76) of the frequency distributions of protrusions/depressions of the surface of aluminum (90 nm) and its alloy with manganese (80 nm) characterizes thicker film coatings that have high irregularities with shallow depressions. The fact that the values of the kurtosis coefficient R_{ku} of the films are above 3 indicates a sharp peak in the frequency distribution of local maxima and minima when the great-

Table 3. Values of the simulation parameters approximating the distribution histograms of particles of the microdroplet fraction over size groups on the surface of films of aluminum and Al–2.1 at % Mn and Al–1.4 at % Ni alloys deposited onto glass (Fig. 6)

Material		OriginPro							
sample	t, h	z_{max}, μm	z_c, μm	$\langle z \rangle$, μm	f_{max}, %	A, a.u.	σ, μm	CV, %	COD (R^2)
Al	10.0	0.43	0.55	0.61	27.88	16.24	0.31	31.17	0.95
Al–Mn	9.1	0.44	0.76	1.27	16.97	19.90	1.70	41.26	0.84
Al–Ni	6.0	0.23	0.34	0.48	27.30	16.14	0.39	40.48	0.98

est concentration of structural components is observed near the middle line of the profile. The surface relief of the Al–Mn alloy film is characterized by the largest kurtosis value ($R_{ku} = 15.64$). Such behavior of the dependence means that pointed protrusions are formed along with filling the cavities during prolonged film deposition. This process prevails over the smoothing of large peaks and can be explained by the formation of a submicrometer conical morphology. Since the distribution with the skewness value close to 2 in most cases is acceptable to consider a normal distribution [40], the nanorelief of films of aluminum and its alloys obtained by the SIAD method can generally be considered as an implementation of a random normal process. Hence, it is necessary to take into account the surface characteristics of the used glass substrate among the factors determining the structure formation in deposited aluminum films. The reason for the rather high kurtosis values of the film profiles may be the sensitivity of this parameter to individual protrusions/depressions.

It should additionally be noted that the alloying of aluminum leads to a decrease in the size spread of structural components of the film surface on a nanometer scale, since the root-mean-square deviation σ determined by approximating the $f(z)$ frequency polygons decreases by a factor of 1.4 (Table 2). The same variance in the distribution of local maxima and minima is a distinctive feature of the morphology of the alloy films. As can be seen from Fig. 7a, the hybrid research parameter behaves nonmonotonically during film deposition with a change in the roughness and has a maximum for the Al–Mn alloy. It is well known that both amplitude parameters R_a and R_{10z} are linearly correlated, but the dependence of k on R_a is not a linear one. This indicates that if the surface of the Al–Ni alloy film is characterized by a sufficiently high density of small structural components, then prolonged (up to 9.1 h) ion-assisted deposition of the Al–Mn alloy leads not only to the formation of a cone-shaped morphology, but also to a decrease in the distance between the relief-profile irregularity protrusions in comparison with other films (Fig. 1).

The analytically obtained plots given in Fig. 4 show a substantial change in the probabilistic characteristics of the roughness parameters upon the transition from the profile assessment to the topographic one. The high degree of reliability of microtopographic parameters is determined by the fact that the basal area of a rough surface is the most informative region in comparison with a single surface section within the basal length. According to the results of profiling the films of aluminum and its alloys, step λ_a of roughness irregularities (wavelengths) is 3.9 μm on average and, consequently, the maximum spatial frequency equal to the reciprocal value of λ_a in magnitude [41] is 0.25 μm^{-1}. It is well known [41] that there must be at least two readings for each oscillation cycle when discretizing a continuous function to avoid losing information about its spectral composition. It follows from the published data [41, 42] that the discretization step in the analysis should not exceed $\lambda_a/2$. Since the film surfaces can be considered uniform and isotropic (at least, within the basal length), and the profiling can be conducted in different directions, we obtain the following condition, the fulfilment of which ensures the reliability of profiling results when measuring a set of amplitude and step roughness parameters: step Δy in the analytical topographic analysis is limited to 2 μm. This confirms the validity of choosing the movement step equal to $\Delta y = 2$ μm (Fig. 2a) when specifying the profiling trajectories at the preliminary stage of applying the proposed algorithm for analyzing the relief of a topographic surface map by using a digitized AFM image of the films.

Thus, a comparison of the microtopographic surface parameters in the longitudinal and transverse directions and an analysis of the surface density and sizes of large-scale inhomogeneities, i.e., particles of the microdroplet fraction, show that the degree of morphological inhomogeneity of the alloy film surfaces, including the volume fraction of microparticles (Fig. 7b), decreases as a result of alloying. According to the theory of nucleation and growth of films [43], the size of stable nuclei inversely depends on the melting temperature of the metal. No considerable dependence of the size of the microdroplet fraction on the melting temperature of the material (660.4°C for Al, 693.7°C for the Al–2.1 at % Mn alloy, and 658.3°C for the Al–1.4 at % Ni alloy [44]) was observed in the experiments. It should be noted that the growth rate of the volume fraction of particles of the microdroplet

fraction during film deposition is approximately six times lower than the rate of increasing the arithmetic-mean roughness of the film with an increase in the deposition time to 10 h (see Figs. 7a and 7b for the values of coefficient a of a positive linear dependence of type $y = ax + b$). The linear nature of the correlation of the arithmetic-mean surface roughness and the volume fraction of microdroplets with the time of film deposition in Fig. 7c indicates a considerable contribution of the surface microroughness caused by microdroplets to the surface topography. However, the presence of microparticles of the coating deposited onto the substrate on the film surface does not lead to frequency distribution bimodality (Fig. 5), as might be expected if the process of film formation is geometrically determined. This means that the morphology of thin metallic films based on aluminum is determined mainly by their growth mechanism discussed above.

Much attention is paid to the problem of wetting rough surfaces, since the model of an ideally smooth and chemically homogeneous surface is rarely applicable to the description of real surfaces. The contact angle is a macroscopic parameter and an integral characteristic of the hydrophilicity/hydrophobicity of the surface of the solid phase. The stronger the interaction between the particles of a liquid and the particles that make up the surface of a solid body, the more favorable the conditions for wetting and the more efficiently the surface adsorbs water molecules. As was found from the experiments performed, the size of a drop of distilled water is many times larger than the characteristic size of the detected nanoscale and microsized topographic inhomogeneities on the surface of films of aluminum and its alloys, which makes it possible to consider the contact angle to be constant along the contact line of the liquid and solid phases. It is well known [45], that the minimum contact angle can be achieved on silicate glass when various types of glass are wetted with water. The equilibrium contact angle measured in this study for distilled water droplets on a glass substrate ($\theta = 22°$) is in good agreement with the published data for silicate glass [45]. The results shown in Table 1 demonstrate that the wetting of the coating–substrate system decreases when a coating in the form of films of aluminum and its binary alloys with manganese or nickel is deposited onto the glass substrate by the SIAD method, and depends on both the topography and the elemental composition of the surface. In particular, it was found that an increase in the surface roughness of the films during prolonged film deposition leads to the greater spreading of a water drop and to a logical decrease in the equilibrium contact angle. Therefore, the equilibrium state of a drop on a rough surface of films of aluminum and its alloys is described by the Wenzel–Derjaguin model [46]. Figure 7a clearly illustrates the operation of the homogeneous regime of wetting of the films with water: in the steady Wenzel state, relief smoothing increases the contact angle of the hydrophilic surface, i.e., impairs wetting. There is no direct correlation between the equilibrium wetting angle and hybrid coefficient k for films of aluminum and its binary alloys with manganese and nickel. This means that the liquid, which is in contact with nanoscale and microsized surface irregularities, fills all the nanorelief cavities of the films and easily penetrates into surface depressions regardless of the shape of profile irregularities.

As mentioned above, the contact angle can also be considered as a parameter useful for estimating the surface free energy of films, which is a function of the surface state. At the same time, modern studies show that alloying allows one to influence the wetting of the sample surface by promoting its hydrophobization or hydrophilization [47, 48], since the free surface energy of a metal that has dispersion and polar structural components changes when additives are introduced. The contact angle is higher for surfaces with low energy [28, 46, 49]. Due to their nature, metals are characterized by high surface energy values (in particular, 865 mN/m for aluminum compared to 20 mN/m for a glass substrate). Therefore, it can be expected that water that has a low surface energy (72 mN/m) should spread well on the surface of the investigated ion-deposited films of aluminum and its alloys. However, it was found that their degrees of wetting are lower than expected when considering the dependence of the hydrophilization of the wetted surface of the films on their composition. The samples are characterized by equilibrium contact angles that range from 73° to 82°, which are several times higher than those for aluminum samples [50–53]. The found contradiction means that the equilibrium contact-angle value of the studied surfaces is influenced by physical and chemical factors that reduce the free surface energy of the films. First, the presence of hydrogen, carbon, and oxygen in the coatings produced by the ion-assisted deposition of metals [54] obviously causes a decrease in the hydrophilic properties of the films. Some of the hydrogen, carbon, and oxygen atoms remain in the unbound state [54]. The source of these impurities in the films is the residual atmosphere of the vacuum chamber, which contains volatile hydrocarbon fractions from the vacuum oil of the diffusion pump. An increase in the free surface energy after cleaning the face-centered cubic (fcc) surface of metals, including the case without a change in the surface roughness during treatment, was reported in [55]. Secondly, the authors of [34, 53, 56, 57] explain the deterioration of the wetting of aluminum materials by water when contact angles θ lie in the range of 70°–90° by the formation of an oxide–hydroxide layer on the surface of the samples in air, since the contact-angle value obtained upon wetting of a coating with an aqueous drop also depends on the concentration of OH groups on the surface. Moreover, attention should be paid to the fact that an Al–Ni alloy film on the surface substantially reduces the hydrophilicity of the thin film–substrate system formed during ion-assisted deposition. On the

contrary, the deposition of an Al–Mn alloy film instead of aluminum on a glass substrate does not lead to any considerable change in the hydrophilicity of the system under study. This indicates that the formation of a protective layer on the aluminum surface is substantially influenced by alloying elements of the alloy. The alloying additives can be concentrated in the surface layer of the resulting aluminum foils when the alloys are synthesized under nonequilibrium conditions (for example, through high-speed crystallization by the method of centrifugal quenching of the melt) [58], thereby increasing their resistance to oxidation. From this point of view, the results obtained previously for rapidly solidified Al–Mn and Al–Ni binary alloys are of particular interest [59, 60], according to which the surface of the synthesized foils is depleted in manganese, but enriched in nickel. Studies of rapidly solidified foils of pure aluminum and Al–Cr alloys, in which the surface regions of the samples are depleted in the alloying element (chromium), just as in the case of Al–Mn alloys, by photoelectron spectroscopy with use of synchrotron radiation confirmed that the composition of the oxide film includes gibbsite γ-$Al(OH)_3$, diaspore α-AlOOH, and boehmite γ-AlOOH [61]. Moreover, highly dispersed inclusions (possibly clusters) of chromium are unevenly distributed over the surface of the foils, near which aluminum and chromium are predominantly present in the metallic state. This indicates that the complex behavior of the contact-angle changes upon the transition from a pure aluminum film to films of its binary alloys can be associated with chemical inhomogeneity of the sample surface. The wetting is inhomogeneous (mixed) in nature when a water drop is in contact with the surface containing heterogeneous regions with different wettability and follows a heterogeneous mechanism [62, 63]. However, studies of recent years have shown that theoretical investigations in this field face difficulty in determining the fraction of a solid wetted with water upon contact with a drop when the topography of its surface is taken into account, which complicates the analysis of the wetting phenomenon for nanoscale and microsized systems. A review of unresolved issues and problems of wetting, including consideration of the factors that may affect the mechanism of wetting of the surface of real bodies, is beyond the scope of this study. These issues were the subject of a number of reviews, for example, [64]. Therefore, the issues of determining the role of the composition and chemical state of the surface of metallic materials (in particular, the ones based on aluminum) in the implementation of homogeneous/heterogeneous wetting regimes upon contact with aqueous media remain poorly understood, and they are specially being analyzed from fundamental and applied points of view.

Thus, the results obtained in this study indicate a strong correlation of the equilibrium contact angle depending on the chemical composition of the material of films deposited onto glass substrates by the SIAD method with both the nanorelief roughness parameters and the physical-chemical state of the heterophase surface of the samples. To determine the elemental composition of the inhomogeneous structure of the oxide–hydroxide layer on the surface of films of aluminum and its alloys, additional studies are required, which are planned to be carried out in the future by the Rutherford backscattering method. The structure formation patterns found in this study for aluminum films during alloying can be used to control the properties of thin-film structures (in particular, to predict their wettability) and are in good agreement with the preliminary data obtained for thin films of Al–Cr and Al–Fe alloys in [27, 65]. The obtained results indicate that it is promising to continue studying the relationship between the roughness parameters and the physical-chemical properties of films formed during ultrafast crystallization on glass substrates by modifying the composition of the coatings and the conditions of ion-assisted deposition.

CONCLUSIONS

Comparative studies of the surfaces of thin films of aluminum and its binary alloys with manganese and nickel by the AFM and SEM methods have made it possible to evaluate the dependences of the structural uniformity of the films on their composition and the time of deposition on a glass substrate with assistance by their self ions and to reveal the correlation between the topographic parameters and surface-structure components, such as microdroplet fraction particles from vacuum-arc-discharge plasma. The frequency distributions are fitted using standard statistical methods in the OriginPro mathematical software package. The AFM images show the film surface with island structures. The arithmetic-mean roughness of coatings varies in the range of 17–32 nm. The statistical processing of the transverse and lateral sizes of the surface-relief components of metallic films has made it possible to determine a set of transverse, longitudinal, and complex parameters for assessing the roughness of the surface and its local microstructure. The experimental distribution functions of the protrusions and depressions of the film-surface nanorelief are unimodal in nature and are in satisfactory agreement with the Gaussian distribution. The frequency distributions of the microdroplet fraction over the particle sizes are lognormal functions. It is established that the degree of morphological surface inhomogeneity of the alloy films compared to films of pure aluminum decreases with the formation of a submicrometer cone-shaped morphology. With prolonged deposition, the number of microparticles on the surface of the samples decreases with an increase in the diameter. The alloy films are characterized by a spread of microdroplets in size. The change in the arithmetic-mean roughness of the films as a function of the volume fraction of microdroplets is described by a positive linear dependence.

The described approach has made it possible to reveal the dependence of the film-surface topography on the structure of the glass substrate and to study the effect of surface inhomogeneities on the wetting properties of the synthesized hydrophilic coatings. In particular, hybrid parameter k calculated with the use of AFM tools during analysis of the sample surface-roughness profiles to estimate the shape of irregularities can be used as a parameter that characterizes the wetting of films with water. The methodology proposed for determining the parameters of the surface structure with application of the analytical profile and topographic analysis of AFM images of films of aluminum and its alloys can be adapted for implementation in the software packages used in industrially produced devices and is suitable for quantitative analysis of the morphology and topography of samples in the nanometer and micrometer ranges.

ACKNOWLEDGMENTS

We are grateful to O.G. Bobrovich (Belarusian State Technological University), S.V. Gusakova (Interuniversity Scientific Research Service Center, Belarusian State University), and Yu.S. Yakovenko (Belorusian State Pedagogical University) for their assistance in preparing the samples by the SIAD method and for SEM and AFM measurements.

FUNDING

This study was performed within the framework of the State research program Physical Materials Science, New Materials, and Technologies (2016–2020, subprogram Materials Science and Technology of Materials, assignment no. 1.40, State registration no. GR 20161123).

CONFLICT OF INTEREST

We declare that we have no conflicts of interest.

REFERENCES

1. S. O. Mbam, S. E. Nwonu, O. A. Orelaja, U. S. Nwigwe, and X.-F. Gou, Mater. Res. Express **6**, 122001 (2019). https://doi.org/10.1088/2053-1591/ab52cd
2. M. Mozetic, A. Vesel, G. Primc, et al., Thin Solid Films **660**, 120 (2018). https://doi.org/10.1016/j.tsf.2018.05.046
3. N. V. Kholodkova and I. V. Kholodkov, Elektrom. Obrab. Mater. **52** (5), 75 (2016).
4. V. F. Gremenok, M. S. Tivanov, and V. B. Zalecskii, *Solar Cells Based on Semiconductor Materials* (Beloruss. Gos. Univ., Minsk, 2007) [in Russian].
5. I. V. Antonets, E. A. Golubev, and V. I. Shcheglov, J. Surf. Invest.: X-ray, Synchrotron Neutron Tech. **15**, 615 (2021).
6. V. G. Bozhkov, N. A. Torkhov, I. V. Ivonin, and V. A. Novikov, Semiconductors **42**, 531 (2008).
7. A. K. Ostapchuk, E. M. Kuznetsova, and A. G. Mikhalishchev, Zaural. Nauchn. Vest., No. 2(6), 15 (2014).
8. I. V. Antonets, L. N. Kotov, S. V. Nekipelov, and E. A. Golubev, Tech. Phys. **49**, 306 (2004).
9. I. V. Antonets, E. A. Golubev, and L. N. Kotov, Poverkhn.: Rentgenovskie, Sinkhrotronnye Neitr. Issled., No. 8, 65 (2007).
10. A. O. Zaitseva, Aktual. Probl. Aviatsii Kosm. **2**, 83 (2015).
11. N. Yu. Sdobnyakov, A. S. Antonov, and D. V. Ivanov, *Morphological Characteristics and Fractal Analysis of Metal Films on Dielectric Surfaces* (Tver, 2019) [in Russian].
12. V. E. Sergeev, V. M. Vorotyntsev, T. S. Sazanova, I. V. Vorotyntsev, and S. V. Kononov, J. Surf. Invest.: X-ray, Synchrotron Neutron Tech. **14**, 875 (2020). https://doi.org/10.1134/S1027451020050183
13. L. E. Afanasieva, V. V. Izmailov, and M. V. Novoselova, J. Surf. Invest.: X-ray, Synchrotron Neutron Tech. **15**, 471 (2021). https://doi.org/10.1134/S1027451021030022
14. V. V. Izmailov and M. V. Novoselova, Vestn. Gos. Tver. Tekh. Univ., Ser. Nauki Tekh., No. 3(7), 5 (2020). https://doi.org/0.46573/2658-5030-2020-3-5-13
15. A. Ya. Grigor'ev, *Physics and Microgeometry of Technical Surfaces* (Belaruskaya Navuka, Minsk, 2016).
16. V. V. Izmailov, L. E. Afanas'eva, and M. V. Novoselova, Mekh. Fiz. Protsessov Poverkhn. Kontakte Tverd. Tel, Detalei Tekhnol. Energ. Oborud., No. 13, 4 (2020).
17. B. Lu and N. Li, Appl. Surf. Sci. **326**, 168 (2015). https://doi.org/10.1016/j.apsusc.2014.11.138
18. K. J. Kubiak, M. C. T. Wilson, T. G. Mathia, and P. Carval, Wear **271**, 523 (2011). https://doi.org/10.1016/j.wear.2010.03.029
19. P. Sigmund, Appl. Phys. Lett. **25** 169 (1974). https://doi.org/10.1063/1.1655425
20. I. S. Tashlykov and I. M. Belyi Belarus Patent No. 2324, Byull. Gos. Patent. Vedomstva Resp. Belarus, No. 1, 30 (1999).
21. G. Karter, D. Kolligon, and I. S. Tashlykov, Perspekt. Mater., No. 1, 5 (1999).
22. A. J. McEvoy, L. Castaner, T. and Markvart, *Solar Cells: Materials, Manufacture and Operation* (Academic, Amsterdam, 2013).
23. M. Garcia-Mendez, S. Morales-Rodrigues, R. Machorro, and W. de la Cruz, Rev. Mex. Fis. **54**, 271 (2008).
24. U. Rau and H. W. Schock, in *Clean Electricity from Photovoltaics*, Ed. by M. D. Archer and M. A. Green (Imperial College Press, London, 2001), p. 277.
25. I. I. Tashlykova-Bushkevich, E. S. Moiseichik, R. D. Lobach, and D. V. Sukhodol'skii, *Materials and Structures of Modern Electronics: Proc. VIII Int. Sci. Conf.* (Minsk, 2018), p. 111.
26. I. I. Tashlykova-Bushkevich, Yu. S. Yakovenko, E. S. Moiseichik, and A. I. Beida, *Current Problems of Solid State Physics: Proc. VIII Int. Sci. Conf.* (Minsk, 2018), Vol. 1, p. 170.
27. I. Tashlykova-Bushkevich, A. Izmailovich, I. Stoliar, A. Ahkapkina, and A. Derkach, *Interaction of Radiation with a Solid Body: Proc. 14th Int. Conf.* (Minsk, 2021), p. 396.

28. A. V. Rudakova and A. V. Emeline, Colloid J. **83**, 20 (2021).
29. A. A. Suslov, V. V. Chikunov, D. I. Shasholko, and S. A. Chizhik, *Proc. VI Belarus. Workshop on Scanning Probe Microscopy* (Minsk, 2004), p. 123.
30. SurfaceXplorer. http://microtm.com/sx/sxr.htm.
31. L. I. Eksler, *Metrological and Technological Studies of Surface Quality* (Zinatne, Riga, 1976) [in Russian].
32. M. Raposo, Q. Ferreira, and P. A. Ribeiro, Mod. Res. Educ. Top. Microsc. **1**, 758 (2007).
33. S. A. Saltykov, *Stereometric Metallography* (Metallurgiya, Moscow, 1976) [in Russian].
34. I. I. Tashlykova-Bushkevich, Yu. S. Yakovenko, V. G. Shepelevich, and I. S. Tashlykov, Fiz. Khim. Obrab. Mater., No. 3, 65 (2016).
35. A. V. Novak and V. R. Novak, Tech. Phys. Lett. **39**, 858 (2013).
36. J. P. Gailliard, in *Surface Engineering* (Springer, Dordrecht, 1984), p. 32. https://doi.org/10.1007/978-94-009-6216-3_2
37. W. Kurz, M. Rappaz, and R. Trivedi, Int. Mater. Rev. **66**, 30 (2020). https://doi.org/10.1080/09506608.2020.1757894
38. S. G. Agababov and L. I. Eksler, Teplofiz. Vys. Temp. **9**, 522 (1971).
39. J. A. Venables G. and D. T. Spiller, in *Surface Mobilities on Solid Materials* (Springer, Boston, 1983), p. 341. https://doi.org/10.1007/978-1-4684-4343-1_16
40. A. Nasledov, IBM SPSS Statistics 20 and AMOS: Professional Statistical Data Analysis (Peter, St. Petersburg, 2013).
41. J. S. Bendat and A. G. Piersol, *Random Data: Analysis and Measurement Procedures* (Wiley, New York, 1971; Mir, Moscow, 1989).
42. V. V. Izmailov and M. V. Novoselova, Fiz.-Khim. Aspekty Izucheniya Klasterov, Nanostrukt. Nanomater., No. 13, **457** (2021). https://doi.org/10.26456/pcascnn/2021.13.457
43. *Handbook of Thin Film Technology*, Ed. by L. I. Maissel and R. Glang (McGraw–Hill, New York, 1970; Sovetskoe Radio, Moscow, 1977).
44. L. F. Mondolfo, *Aluminum Alloys: Structure and Properties* (Elsevier, Amsterdam, 1976; Metallurgiya, Moscow, 1979).
45. A. D. Zimon, *Liquid Adhesion and Wetting*(Khimiya, Moscow, 1974) [in Russian].
46. L. B. Boinovich, Her. Russ. Acad. Sci. **83**, 8 (2013). https://doi.org/10.1134/S1019331613010024
47. V. V. Chebodaeva, E. G. Komarova, Yu. P. Sharkeev, A. V. Rudakova, and A. V. Emelin, Kolloid. Zh. **83**, 3 (2021). https://doi.org/10.31857/S0023291221010109
48. F. Thomsen, Adhes. Adhes. Sealants **10** (4), 12 (2013). https://doi.org/10.1365/s35784-013-0230-1
49. A. V. Emeline, A. V. Rudakova, M. Sakai, T. Murakami, and A. Fujishima, J. Phys. Chem. **117**, 12086 (2013). https://doi.org/10.1021/jp400421v
50. W. Liu, L. Sun, Y. Luo, R. Wu, H. Jiang, Y. Chen, G. Zeng, and Y. Liu, Appl. Surf. Sci. **280**, 193 (2013). https://doi.org/10.1016/j.apsusc.2013.04.124
51. P. Bizi-Bandoki, S. Benayoun, S. Valette, B. Beaugiraud, and E. Audouard, Appl. Surf. Sci. **257**, 5213 (2011). https://doi.org/10.1016/j.apsusc.2010.12.089
52. C. Lee, H. Cho, D. Kim, and W. Hwang, Appl. Surf. Sci. **288**, 619 (2014) https://doi.org/10.1016/j.apsusc.2013.10.084
53. I. I. Tashlykova-Bushkevich, V. G. Shepelevich, M. Amati, L. Gregoratti, and M. Kiskinova, J. Surf. Invest.: X-ray, Synchrotron Neutron Tech. **14**, 66 (2020). https://doi.org/10.1134/S102745102001019X
54. O. G. Bobrovich, I. S. Tashlykov, V. V. Tul'ev, and S. M. Baraishuk, Fiz. Khim. Obrab. Mater., No. 1, 54 (2006).
55. V. S. Ripenko, M. V. Erofeev, M. A. Shulepov, and V. F. Tarasenko, Izv. Vyssh. Uchebn. Zaved., Fiz. **59** (9), 252 (2016).
56. M. Rahimi, P. Fojan, L. Gurevich, and A. Afshari, Appl. Surf. Sci. **296**, 124 (2014). https://doi.org/10.1016/j.apsusc.2014.01.059
57. B. Lu and N. Li, Appl. Surf. Sci. **326**, 168 (2015). https://doi.org/10.1016/j.apsusc.2014.11.138
58. I. I. Tashlykova-Bushkevich V. and G. Shepelevich, J. Alloys Compd. **299**, 205 (2000). https://doi.org/10.1016/S0925-8388(99)00750-1
59. I. I. Tashlykova-Bushkevich, J. Alloys Compd. **478**, 229 (2009). https://doi.org/10.1016/j.jallcom.2008.12.006
60. I. I. Tashlykova-Bushkevich, *Rapidly Hardened Materials and Coatings: Proc. 3rd All-Russian. Sci.-Tech. Conf.* (Moscow, 2004), p. 23.
61. I. I. Tashlykova-Bushkevich, M. Amati, B. Aleman, H. Sezen, L. Gregoratti, and M. Kiskinova, Int. J. Hydrogen Energy **41**, 9100 (2016). https://doi.org/10.1016/j.ijhydene.2016.03.193
62. J. N. Israelachvili and M. L. Gee, Langmuir **5**, 288 (1989). https://doi.org/10.1021/la00085a059
63. J. Wang, D. Bratko, and A. Luzar, Proc. Natl. Acad. Sci. U. S. A. **108**, 6374 (2011). https://doi.org/10.1073/pnas.1014970108
64. J. W. Drelich, L. Boinovich, E. Chibowski, C. D. Volpe, L. Holysz, A. Marmur, and S. Siboni, Surf. Innovations **8**, 3 (2020). https://doi.org/10.1680/jsuin.19.00007
65. I. I. Tashlykova-Bushkevich, J. S. Yakovenko, I. and A. Bushkevich, Int. J. Nanosci. **18**, 1940062 (2019). https://doi.org/10.1142/S0219581X19400623

Translated by O. Kadkin